

The elastic constants of solid ^4He under pressure: a diffusion Monte Carlo study

C. Cazorla^a, Y. Lutsyshyn^b and J. Boronat^c

^a *Institut de Ciència de Materials de Barcelona (ICMAB-CSIC), 08193 Bellaterra, Spain*

^b *Institut für Physik, Universität Rostock, 18051 Rostock, Germany*

^c *Departament de Física i Enginyeria Nuclear,*

Universitat Politècnica de Catalunya,

Campus Nord B4-B5, E-08034, Barcelona, Spain

Abstract

We study the elasticity of perfect ^4He at zero-temperature using the diffusion Monte Carlo method and a realistic semi-empirical pairwise potential to describe the He-He interactions. In particular, we calculate the value of the elastic constants of hcp helium $\{C_{ij}\}$ as a function of pressure up to ~ 110 bar. It is found that the pressure dependence of all five non-zero $\{C_{ij}\}$ is linear and we provide an accurate parametrization of each of them. Our elastic constants results are compared to previous variational calculations and low-temperature measurements and in general we find notably good agreement among them. Furthermore, we report $T = 0$ results for the Grüneisen parameters, sound velocities and Debye temperature of hcp ^4He . This work represents the first of a series of computational studies aimed at thoroughly characterizing the response of solid helium to external stress-strain.

PACS numbers: 67.80.-s, 02.70.Ss, 67.40.-w

I. INTRODUCTION

The behavior of solid ^4He , and of quantum crystals in general (e.g., H_2 and Ne), is exceptionally so rich that despite having been investigated for more than about eight decades is to this day not yet completely understood. One example of helium's intriguing nature is its elasticity. Experimental studies on the elastic properties of hcp ^4He were already conducted by Wanner, Crepeau and Greywall in the early seventies.¹⁻³ Those original works consisted of series of sound-velocity measurements performed at thermodynamic conditions relatively close to the stability domain of the liquid, namely $T \sim 1$ K and $25 \leq P \leq 50$ bar. With the advance of time and technology cryogenic and crystal growth techniques have been improved so notably that at present is possible to analyze practically defect-free ^4He samples at just few mK in the laboratory. Recently, Beamish and collaborators have developed a new experimental technique that has allowed them to measure directly the shear modulus μ of hcp ^4He under extremely low strains and frequencies.^{4,5} The temperature dependence of μ within the temperature interval $0.5 \leq T \leq 0.01$ K has been determined and a striking resemblance with non-classical rotational inertia (NCRI) data obtained in torsional oscillator experiments^{6,7} has been unravelled. Specifically, the value of the NCRI and shear modulus of helium increases about 2 % as the temperature is lowered down to 0.01 K. Despite Beamish *et al.*'s findings have been initially rationalized in terms of pinning (unpinning) of dislocations induced by the presence of static (mobile) ^3He impurities,^{4,8-10} it remains to be clarified whether the cited experimental similarities must be regarded simply as coincidental or contrarily correspond to manifestations of a same and unique quantum phenomenon known as supersolidity.¹¹⁻¹³

Simulation techniques have been demonstrated as invaluable tools for predicting and accurately characterizing the energetic and structural properties of quantum solids.¹⁴⁻¹⁹ Nevertheless, computational studies on the elasticity of solid ^4He so far have been very infrequent. To the best of our knowledge, there exists only one recent work by Pessoa *et al.* in which the shear modulus of solid helium has been explicitly calculated from first-principles.²⁰ This computational scarcity strongly contrasts with research done in other fields like classical solid state theory and/or high pressure physics, where estimation of the elastic properties of materials (e.g. strain-stress tensor, Grüneisen parameters, vibrational phonon frequencies, etc.) is a standard.²¹⁻²⁴ The likely explanation for such a contrast

(besides no particular enthusiasm in the matter prior to Beamish *et al.* experiments) are the technical difficulties encountered in modeling of bosonic quantum effects, namely atomic delocalization, anharmonicity and particle exchanges. These quantum atomic effects are indeed crucial to comprehend the nature of solid ^4He at low temperatures and, as a matter of fact, customary harmonic and quasi-harmonic computational approaches^{25–27} can not be used to obtain a reliable picture of it.

Here, we present a computational study of the elastic properties of perfect (e.g. free of defects) solid ^4He in the hcp structure based on the diffusion Monte Carlo approach. This work is intended to improve our understanding of how solid helium reacts to external strains/stresses, and further extends the work initiated by Pessoa *et al.*²⁰ In particular, we provide the zero-temperature dependence of helium elastic constants and related quantities (e.g. sound velocities, Grüneisen parameters and the Debye temperature) on pressure up to ~ 110 bar. Our results are compared to experimental data and other calculations whenever is possible and, as it will be shown later on, good agreement among them is generally found. The computational method that we employ is fully quantum and virtually exact (i.e., in principle only affected by statistical uncertainties) so that from a technical point of view our study also represents an improvement with respect to previous first-principles work²⁰ based on variational Monte Carlo calculations (i. e., subjected to statistical and importance sampling biases).

The remainder of the article is as follows. In Section II, we review the basics of elasticity in hcp crystals and provide the details of our computational method and strategy. In the following section, we present our results along with some discussions. Finally, we summarize the main conclusions obtained and comment on prospective work in Section IV.

II. THEORY AND COMPUTATIONAL DETAILS

A. Elastic constants

For small strains, the zero-temperature energy of a crystal can be expressed as

$$E = E_0 + \frac{1}{2}V_0 \sum_{i,j=1}^6 C_{ij}s_i s_j , \quad (1)$$

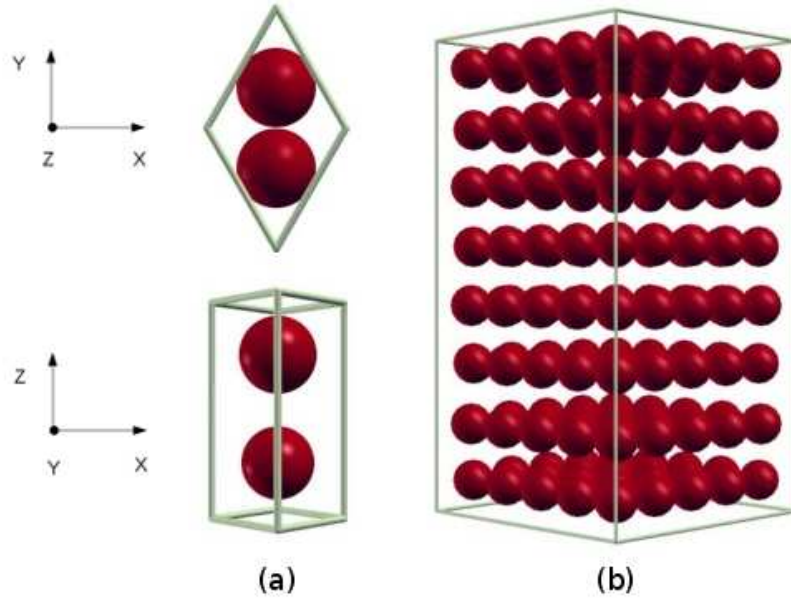


FIG. 1: (a) Representation of the hcp unit cell with primitive translational vectors \mathbf{a}_1 , \mathbf{a}_2 and \mathbf{a}_3 , and two-atoms basis set (see text). (b) Sketch of the 200-atoms supercell used in the pure shear calculations, built by replicating the hcp unit cell $5 \times 5 \times 4$ times along the primitive translational vectors \mathbf{a}_1 , \mathbf{a}_2 and \mathbf{a}_3 , respectively.

where V_0 and E_0 are the volume and internal energy of the undistorted solid, $\{C_{ij}\}$ the elastic constants and $\{s_i\}$ the strain components defined such that s_1 , s_2 and s_3 are fractional increases in the x , y and z directed axes, and s_4 , s_5 and s_6 angular increases of the xy , xz and yz angles.^{28–30} The symmetry properties of the crystal under consideration define the number of elastic constants which are non-zero. For hcp crystals, only five elastic constants are different from zero, namely C_{11} , C_{12} , C_{33} , C_{13} and C_{44} , where C_{44} is commonly known as the shear modulus and abbreviated μ . In order to calculate these five non-zero elastic constants is necessary to compute the second derivative of the internal energy of the crystal with respect to the strain tensor σ_{ij} . For this, the hcp crystal must be first considered in full symmetry, that is, expressed in terms of its unit cell with primitive translational vectors $\mathbf{a}_1 = a \left(+\frac{1}{2}\mathbf{i} + \frac{\sqrt{3}}{2}\mathbf{j} \right)$, $\mathbf{a}_2 = a \left(-\frac{1}{2}\mathbf{i} + \frac{\sqrt{3}}{2}\mathbf{j} \right)$ and $\mathbf{a}_3 = c\mathbf{k}$ (where a and c are the lattice parameters in the basal plane and along the z axis respectively, and \mathbf{i} , \mathbf{j} and \mathbf{k} correspond to the usual unitary Cartesian vectors), and two-atom basis set $\mathbf{r}_1 = \frac{1}{2}\mathbf{a}_1 + \frac{1}{3}\mathbf{a}_2 + \frac{2}{3}\mathbf{a}_3$ and $\mathbf{r}_2 = (0, 0, 0)$ (see Fig. 1).

The relationships between the hcp elastic constants $\{C_{ij}\}$ and applied strain were determined long-time ago within the framework of elasticity theory, those being^{28–30}

$$K = -V \left(\frac{\partial P}{\partial V} \right)_{V=V_0} = \frac{C_{33}(C_{11} + C_{12}) - 2C_{13}^2}{C_{11} + C_{12} + 2C_{33} - 4C_{13}} , \quad (2)$$

$$-V \left(\frac{\partial \ln c/a}{\partial V} \right)_{V=V_0} = \frac{C_{33} - C_{11} - C_{12} + C_{13}}{C_{11} + C_{12} + 2C_{33} - 4C_{13}} , \quad (3)$$

$$C_0 = C_{11} + C_{12} + 2C_{33} - 4C_{13} , \quad (4)$$

$$C_{66} = \frac{1}{2}(C_{11} - C_{12}) \quad (5)$$

and

$$C_{44} = C_{44} . \quad (6)$$

Equations (2) and (3) correspond to homogeneous strains that change the volume and shape of the hcp unit cell. The dependence of pressure P and c/a ratio on volume can be readily obtained from standard equation of state calculations. On the other hand, equations (4), (5) and (6) represent heterogeneous strains that keep the volume of the hcp unit cell unaltered. In order to calculate the value of the pure shears C_0 , C_{66} and C_{44} is necessary to compute the variation of the internal energy of the equilibrium structures with respect to certain deformations, which can be written as transformed primitive translational vectors. In the C_0 case, these are

$$\begin{aligned} \mathbf{a}_1^0 &= a\epsilon^{-1} \left(+\frac{1}{2}\mathbf{i} + \frac{\sqrt{3}}{2}\mathbf{j} \right) \\ \mathbf{a}_2^0 &= a\epsilon^{-1} \left(-\frac{1}{2}\mathbf{i} + \frac{\sqrt{3}}{2}\mathbf{j} \right) \\ \mathbf{a}_3^0 &= c\epsilon^2\mathbf{k} , \end{aligned} \quad (7)$$

where $\epsilon = (1 + \eta)^{1/2}$, $C_0 = \frac{2}{V_0} \left(\frac{\partial^2 E}{\partial \eta^2} \right)_{V=V_0}$ and the equilibrium condition is satisfied at $\eta = 0$. For C_{66} , we have

$$\begin{aligned} \mathbf{a}_1^{66} &= a\gamma^{1/2} \left(+\frac{1}{2}\mathbf{i} + \gamma^{-1}\frac{\sqrt{3}}{2}\mathbf{j} \right) \\ \mathbf{a}_2^{66} &= a\gamma^{1/2} \left(-\frac{1}{2}\mathbf{i} + \gamma^{-1}\frac{\sqrt{3}}{2}\mathbf{j} \right) \\ \mathbf{a}_3^{66} &= c\mathbf{k} , \end{aligned} \quad (8)$$

where $C_{66} = \frac{1}{V_0} \left(\frac{\partial^2 E}{\partial \gamma^2} \right)_{V=V_0}$ and the equilibrium condition is satisfied at $\gamma = 1$. And finally for C_{44} ,

$$\begin{aligned} \mathbf{a}_1^{44} &= a \left(+\frac{1}{2}\mathbf{i} + \frac{\sqrt{3}}{2}\mathbf{j} - \frac{\phi}{2}\mathbf{k} \right) \\ \mathbf{a}_2^{44} &= a \left(-\frac{1}{2}\mathbf{i} + \frac{\sqrt{3}}{2}\mathbf{j} - \frac{\phi}{2}\mathbf{k} \right) \\ \mathbf{a}_3^{44} &= c\mathbf{k} , \end{aligned} \tag{9}$$

where $C_{44} = \frac{1}{V_0} \left(\frac{\partial^2 E}{\partial \phi^2} \right)_{V=V_0}$ and the equilibrium condition is satisfied at $\phi = 0$.

Once the value of the bulk modulus K and quantities $\partial \ln(c/a)/\partial V$, C_0 , C_{66} and C_{44} is determined, one can calculate the five corresponding $C_{ij} \neq 0$ hcp elastic constants straightforwardly by solving the non-linear system of equations defined by Eqs. (2)-(6).

B. Diffusion Monte Carlo

The fundamentals of the diffusion Monte Carlo (DMC) method have been reviewed with detail in other works³¹⁻³³ so for brevity's sake we recall here only the essential ideas.

In the DMC approach, the time-dependent Schrödinger equation of a quantum system of N interacting particles is solved stochastically by simulating the time evolution of the Green's function propagator $e^{-\frac{i}{\hbar}\hat{H}t}$ in imaginary time τ . For $\tau \rightarrow \infty$, sets of configurations (walkers) $\{\mathbf{R}_i \equiv \mathbf{r}_1, \dots, \mathbf{r}_N\}$ rendering the probability distribution function $(\Psi_0\Psi)$ are generated, where Ψ_0 is the true ground-state wave function of the system and Ψ the trial wave function used for importance sampling. Within DMC, virtually exact results (i.e., subjected to statistical uncertainties only) are obtained for the ground-state total energy and related quantities in bosonic quantum systems.³⁴⁻³⁶ It is worth noticing that despite asymptotic DMC values do not depend on the choice of the trial wave function, the corresponding algorithmic efficiency is tremendously affected by the quality of Ψ .

We are interested in studying the ground-state of perfect hcp ^4He , which we assume to be governed by the Hamiltonian $H = -\frac{\hbar^2}{2m_{\text{He}}} \sum_{i=1}^N \nabla_i^2 + \sum_{i<j}^N V_{\text{He-He}}(r_{ij})$ where m_{He} is the mass of an helium atom, N the number of particles and $V_{\text{He-He}}$ the semi-empirical pairwise potential due to Aziz *et al.*³⁷ It is worth noting that this two-body potential provides an excellent description of the He-He interactions, including weak long-ranged van der Waals forces, over all the pressure range considered in this work.^{14,38}

The trial wave function that we use for importance sampling Ψ_{SNJ} simultaneously reproduces crystal ordering and Bose-Einstein symmetry (that is, remains unchanged under the permutation of atoms). This model wave function was recently introduced in Ref. [39] and it reads

$$\Psi_{\text{SNJ}}(\mathbf{r}_1, \dots, \mathbf{r}_N) = \prod_{i < j}^N f(r_{ij}) \prod_{J=1}^N \left(\sum_{i=1}^N g(r_{iJ}) \right), \quad (10)$$

where the index in the second product runs over perfect lattice position vectors (sites). In previous works, we have demonstrated that Ψ_{SNJ} provides an excellent description of the ground-state properties of bulk hcp ^4He ³⁹ and quantum solid films.^{15,19,40} The key ingredient for this progress stays in the Ψ_{SNJ} localization factor (second term in Eq. (10)), which is constructed in such a way that voids originated by multiple occupancy of a same site are energetically penalized. Correlation functions in Eq. (10) were adopted in the McMillan, $f(r) = \exp[-1/2 (b/r)^5]$, and Gaussian, $g(r) = \exp[-1/2 (ar^2)]$, forms. The value of the parameters in factors f and g were optimized variationally at density $\rho = 0.480 \text{ } \sigma^{-3}$ ($\sigma = 2.556 \text{ } \text{\AA}$, $b = 1.08 \text{ } \sigma$ and $a = 10.10 \text{ } \sigma^{-2}$) and kept fixed in the rest of simulations performed at different densities.

The technical parameters in our calculations were set in order to ensure convergence of the total energy per particle to less than 0.02 K/atom. For instance, the value of the mean population of walkers was held to 400 and the length of the imaginary time-step $\Delta\tau$ was $5 \cdot 10^{-4} \text{ K}^{-1}$. Statistics were accumulated over 10^5 DMC steps performed after system equilibration, and the approximation used for the short-time Green's function $e^{-\frac{i}{\hbar} \hat{H} \Delta\tau}$ was accurate up to order $(\Delta\tau)^3$.⁴¹

C. Computational strategy

In order to work out Eq. (2) we used the bulk modulus volume dependence reported in Ref. [42], where the equation of state of perfect hcp ^4He was already calculated employing the DMC method and considering variational finite-size corrections to the total energy.¹⁴ The equilibrium value of the c/a ratio was found to be constant and equal to 1.63(1) over all the pressure range $0 \leq P \leq 110 \text{ bar}$. (This outcome is consistent with previous first-principles results obtained by other authors.⁴³) Consequently, the left-hand side of Eq. (3)

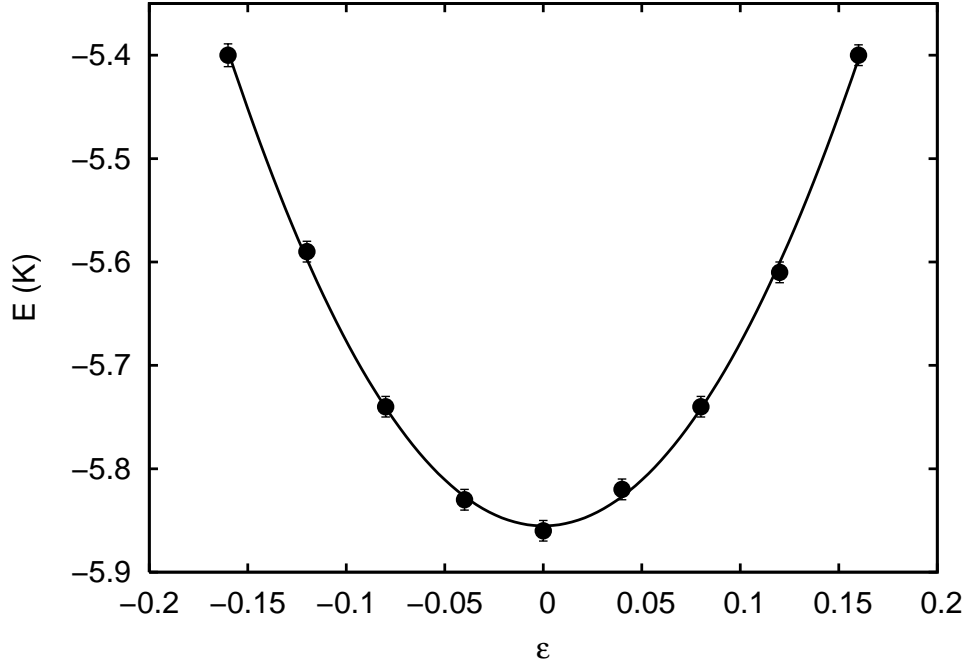


FIG. 2: C_{44} shear energy results obtained in perfect hcp ^4He at density $\rho = 0.480 \text{ } \sigma^{-3}$. The equilibrium value corresponding to the undistorted hcp structure is quoted at $\epsilon = 0$ and the solid line represents a third-order polynomial fit to the energies.

vanishes and the solution to the fifth-order equation system defined by Eqs. (2)-(6) is

$$\begin{aligned}
 C_{11} &= K + C_{66} + \frac{1}{18}C_0 \\
 C_{12} &= K - C_{66} + \frac{1}{18}C_0 \\
 C_{13} &= K - \frac{1}{9}C_0 \\
 C_{33} &= K + \frac{2}{9}C_0 \\
 C_{44} &= C_{44} .
 \end{aligned} \tag{11}$$

The simulation box used in our pure shear calculations contains 200 He atoms and was generated by replicating the hcp unit cell 5 times along the \mathbf{a}_1 and \mathbf{a}_2 directions and 4 times along the c axis (see Fig. 1). In proceeding so, hexagonal symmetry in our supercell calculations is guaranteed by construction. Periodic boundary conditions were imposed along the three directions defining the edges of the non-orthorombic simulation boxes.

The value of the second derivatives involved in Eqs. (4)-(6) were computed following the next strategy. For each volume and pure shear considered, first we calculated the

total energy per particle in a series of supercells generated by incrementally distorting the equilibrium geometry according to the transformed translational lattice vectors (7)-(9). Up to eight different and equally spaced shear increments (e.g., ϵ , γ and ϕ) were considered for each volume, taking both positive and negative values. Subsequently, the series of shear-dependent total energies so obtained at fixed volume were fitted to a third-order polynomial function of the form $f(x) = a + bx^2 + cx^3$. In all the cases, we found that the optimal a , b and c values reproduced the series of calculated total energies per particle within their statistical errors (see Fig. 2). Regarding total energy shifts correcting for the finite-size effects, no variational energy corrections were considered in the pure shear calculations. The reason for this is convenience since finite-size energy corrections are not expected to depend on the small shear distortions considered in this work, and consequently they do not contribute to the value of the second derivatives involved in the calculation of the elastic constants. We shall stress that the volume of the simulation cell in pure shear calculations is kept fixed in contrast to bulk modulus and $\partial \ln(c/a)/\partial V$ calculations, in which accurate finite-size corrections to the energy are certainly required.

III. RESULTS AND DISCUSSIONS

A. Elastic constants

In Figures 3, 4 and 5, we show the pressure dependence of the five elastic constants of perfect hcp ^4He as obtained in our calculations. The error bars δC_{ij} in our results, stemming from both the statistical uncertainties of the energies and corresponding third-order polynomial fits, typically amount to $\delta C_{ij}/C_{ij} \sim 2\%$. We found that the pressure variation of all five elastic constants is practically linear within all the studied range. Consequently, we performed fits of the form $C_{ij}(P) = a_{ij} + b_{ij}P$ to our results (see Figures 3, 4 and 5), and obtained a series of a_{ij} and b_{ij} coefficients that we quote in Table I. We note that average variance values obtained in the reduced- χ^2 tests corresponding to our fits were always smaller than 2.

Comparison between our DMC calculations, previous variational Monte Carlo (VMC) results and experimental data is provided also in Figures 3-5. VMC results reported at $P \sim 34 \text{ bar}^{20}$ have been obtained by Pessoa *et al.* using a shadow wave function model (SWF).⁴⁴

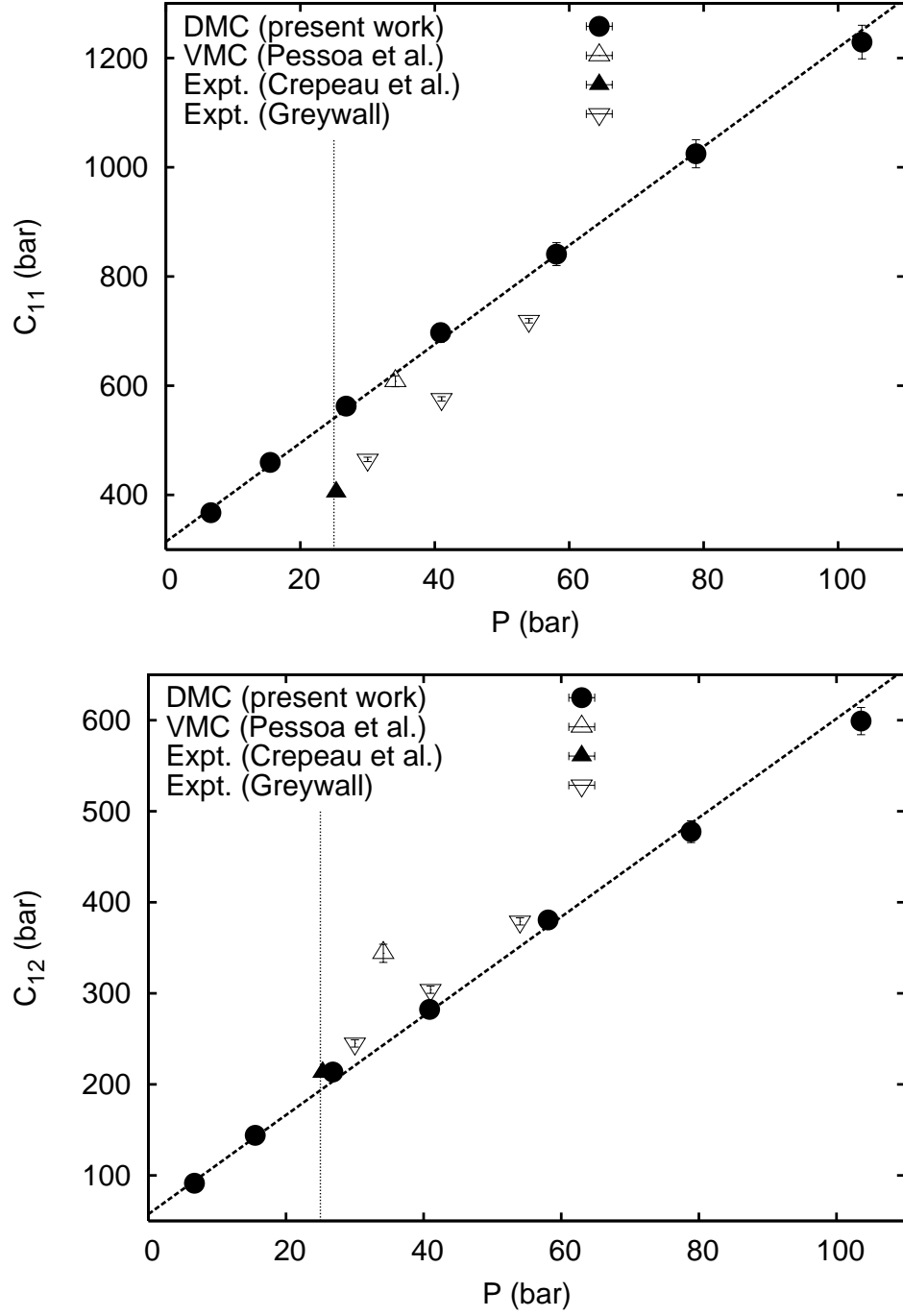


FIG. 3: Zero-temperature C_{11} and C_{12} elastic constants of perfect hcp ^4He as a function of pressure. Previous variational Monte Carlo (VMC) calculations [20] and experimental data [2] [3] are shown for comparison. The vertical dotted line represents the zero-temperature freezing pressure of ^4He and the straight dashed lines are linear fits to the DMC results (see text).

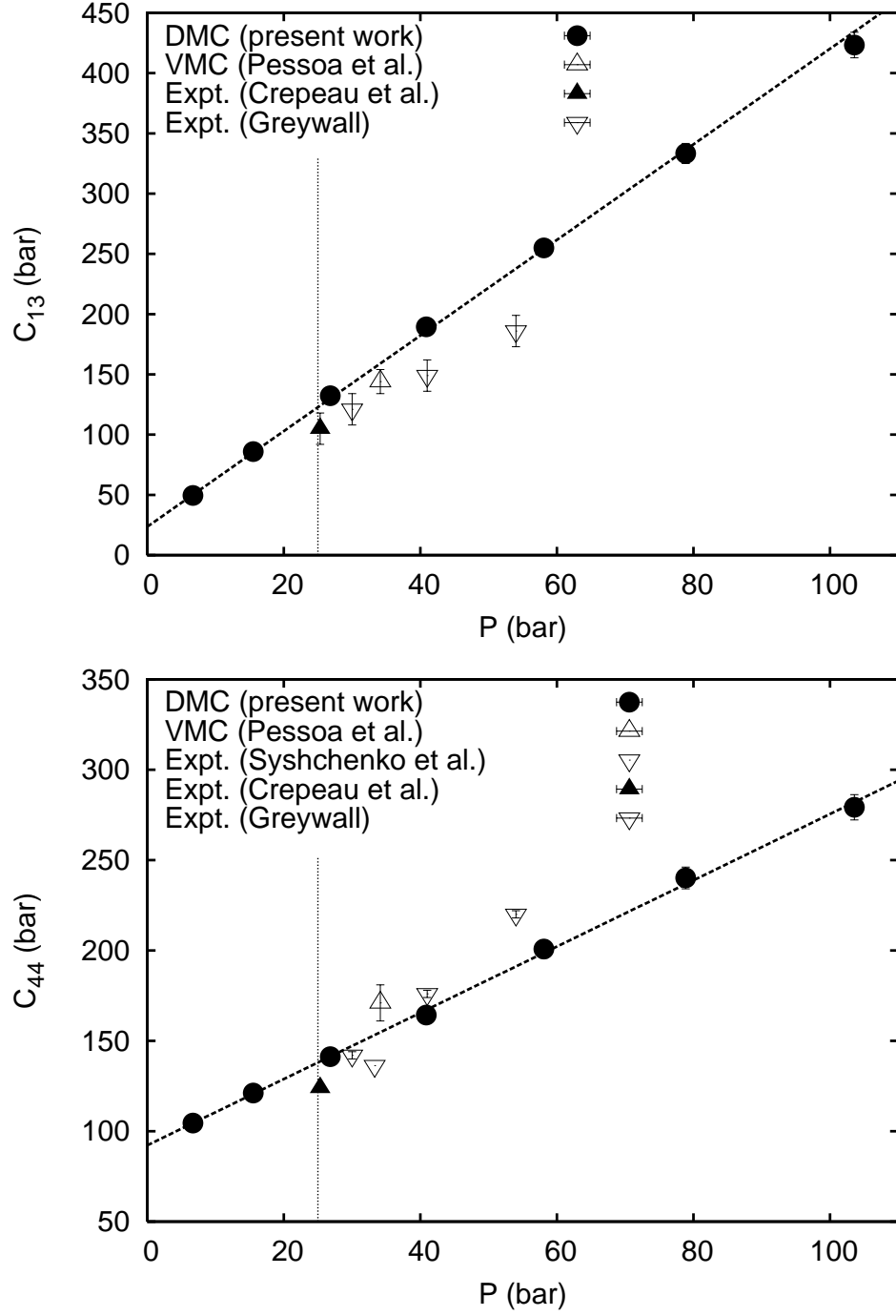


FIG. 4: Zero-temperature C_{13} and C_{44} elastic constants of perfect hcp ^4He as a function of pressure. Previous variational Monte Carlo (VMC) calculations [20] and experimental data [2] [3] [5] are shown for comparison. The vertical dotted line represents the zero-temperature freezing pressure of ^4He and the straight dashed lines are linear fits to the DMC results (see text).

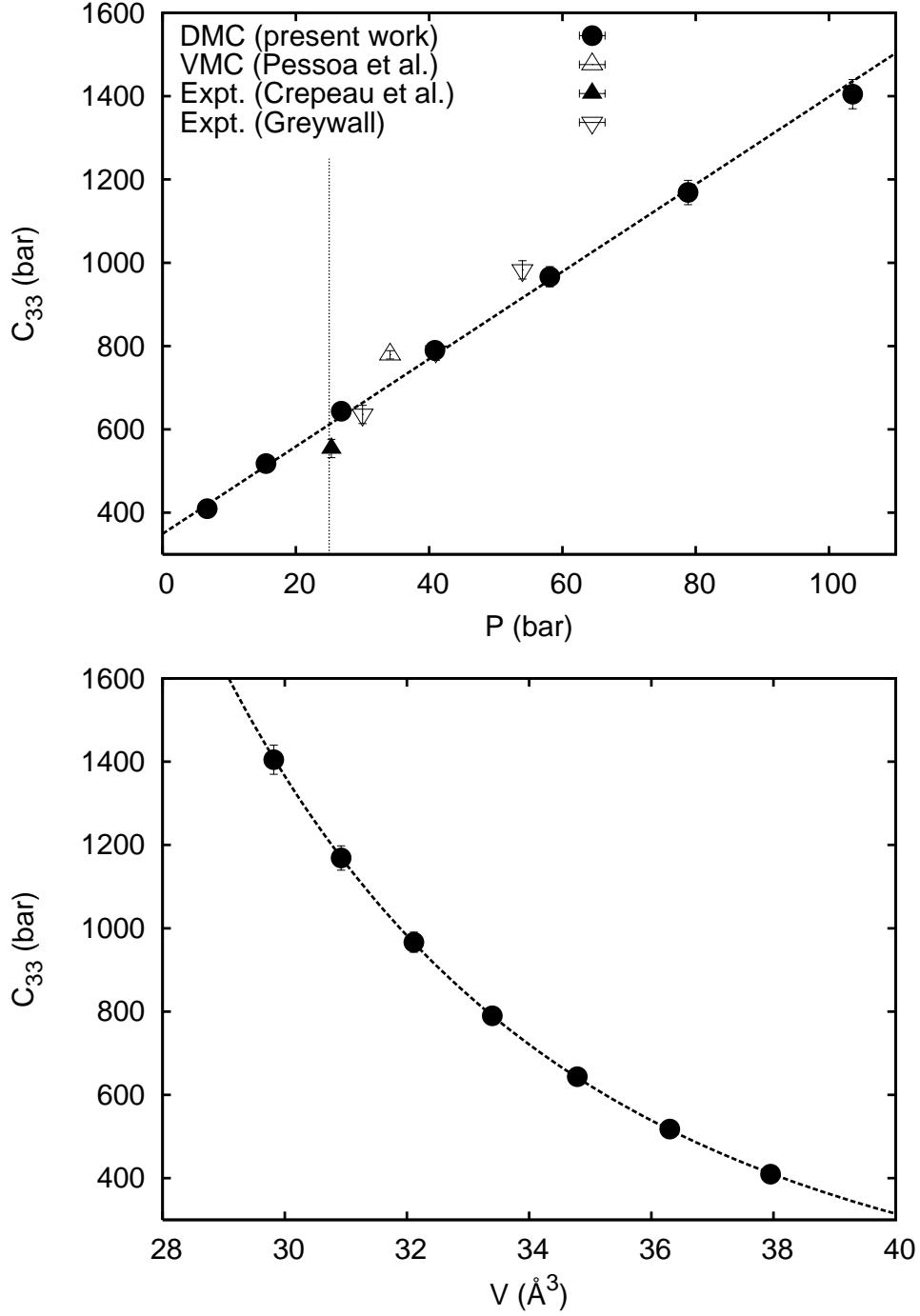


FIG. 5: *Top*: Zero-temperature C_{33} elastic constant of perfect hcp ^4He as a function of pressure. A previous variational Monte Carlo (VMC) calculation [20] and experimental data [2] [3] are shown for comparison. The vertical dotted line represents the zero-temperature freezing pressure of ^4He and the straight dashed line is a linear fit to the DMC results (see text). *Bottom*: Dependence of the C_{33} elastic constant on volume. The dashed line represents a power law fit to the DMC results from which the value of the corresponding Grüneisen parameter is obtained (see text).

	C_{11}	C_{12}	C_{13}	C_{33}	C_{44}
a_{ij}	314.26	57.45	23.59	349.22	92.19
b_{ij}	9.05	5.44	3.97	10.49	1.83

TABLE I: Value of the parameters obtained in the linear fits to our $C_{ij}(P)$ results (see text). a_{ij} 's are expressed in units of bar.

This type of trial wave function correctly accounts for the atomic Bose-Einstein statistics, is translationally invariant and so far it has yielded the most accurate variational description of solid helium.⁴⁵ Arguably, Pessoa's VMC predictions are in fairly good agreement with our DMC results since in general the relation $|C_{ij}^{\text{VMC}} - C_{ij}^{\text{DMC}}|/C_{ij}^{\text{DMC}} \leq 10\%$ is fulfilled. (This inequality is only violated by C_{12} however in that case measurements appear to follow closely our results.) Recalling that evaluation of C_{ij} 's requires from the computation of total energy second derivatives, it can be said that the satisfactory DMC-VMC agreement found further corroborates the excellent variational quality of the SWF model.

Regarding the experimental data taken from Refs. [2,3], we also find good agreement with them (see Figures 3-5). The sound-velocity measurements performed by Crepeau and Greywall involved high-quality single helium crystals whose basal plane orientations were accurately determined using x-rays. Consequently, our modest discrepancies with Crepeau and Greywall's data are very likely to be originated by thermal effects given that the temperature conditions in those experiments were $T \sim 1$ K. Reassuringly, our C_{44} results reproduce closely recent ^4He shear modulus measurements performed by Beamish *et al.* at just few mK (see Figure 4).^{4,5} We will comment again on this issue in Section III B however it can be already claimed that the manifested overall good accordance between our C_{ij} calculations and $30 \leq P \leq 60$ bar experiments appears to endorse the reliability of our computational approach.

Another quantity of interest in the study of crystal elasticity is the Grüneisen parameter $\hat{\gamma}$. Essentially, this parameter quantifies how atomic vibrations in a crystal are affected by changes in volume. This quantity is customarily defined by $\hat{\gamma} = (V/C_v)\beta K$, where C_v stands for the specific heat and β for the coefficient of the thermal expansion. However, this definition is not practical for low temperature calculations since in general quantities

C_v and β tend to zero in a similar trend near $T = 0$, and thus leads to an indetermination. Alternatively, Klein *et al.*⁴⁶ derived a Grüneisen parameter expression that is valid in the zero-temperature limit and which depends on the individual vibrational frequency modes. Specifically, Klein's expression can be reformulated in terms of the elastic constants as³

$$\gamma_{ij} = -\frac{1}{2} \frac{\partial \ln C_{ij}}{\partial \ln V} - \frac{1}{6} . \quad (12)$$

Naturally, the volume dependence of each C_{ij} elastic constant can then be fitted to a function of the form

$$C_{ij}(V) = A \left(\frac{V}{V_0} \right)^{-\left(\frac{1}{3} + 2\gamma_{ij}\right)} , \quad (13)$$

so that one can readily obtain the value of the corresponding γ_{ij} parameter. We proceeded in this way using the C_{ij} results obtained in our $0 \leq P \leq 110$ bar simulations (see Figure 5) and got $\gamma_{11} = 2.34$ (5) , $\gamma_{12} = 3.69$ (5) , $\gamma_{13} = 4.23$ (5) , $\gamma_{33} = 2.70$ (5) and $\gamma_{44} = 1.91$ (5) , where the numerical uncertainties are expressed within parentheses. The averaged Grüneisen parameter $\hat{\gamma} = \frac{1}{5} \sum \gamma_{ij}$ corresponding to our results is 2.67 (5), where the summation runs over indexes 11, 12, 33, 44 and 66 ($\gamma_{66} = 2.70$ as obtained from C_{66}) because the respective elastic constants are the quantities which are directly measured in sound-velocity experiments.³ Our $\hat{\gamma}$ value compares very well with Greywall's experimental result of 2.7, however we note that in our calculations the value of the dispersion $\frac{1}{5} \sum |\gamma_{ij} - \hat{\gamma}|$ is non-zero. It is worth comparing the value of the zero-temperature Grüneisen parameter of solid helium to that of other rare-gas species. We know from Ref. [47] that $\hat{\gamma}$ is 2.5 in Ne, 2.7 in Ar, 2.7 in Kr and 2.5 in Xe. Consequently, the elastic constants of all five noble gases will vary very similarly upon a same volume change. The same conclusion, however, does not apply to pressure since the bulk modulus of each element is appreciably different from that of the others.

In order to quantify the importance of quantum effects in our study, we computed the contribution of the potential and kinetic energies to the shear modulus (C_{44}^p and C_{44}^k , respectively). For this, we carried out simulations at density $\rho = 0.480 \sigma^{-2}$ in which the *exact* value of the second derivative of the potential energy E^p with respect to strain was calculated using the pure estimator technique.³⁶ The kinetic energy contribution to the shear modulus C_{44}^k was subsequently obtained by subtracting the quantity $C_{44}^p = \frac{1}{V_0} \left(\frac{\partial^2 E^p}{\partial \phi^2} \right)_{V=V_0}$ to C_{44} . (We checked that the strain dependence of E^k could also be accurately fitted to a third-order polynomial function). In fact, the $T = 0$ value of C_{44}^k in a classical crystal exactly

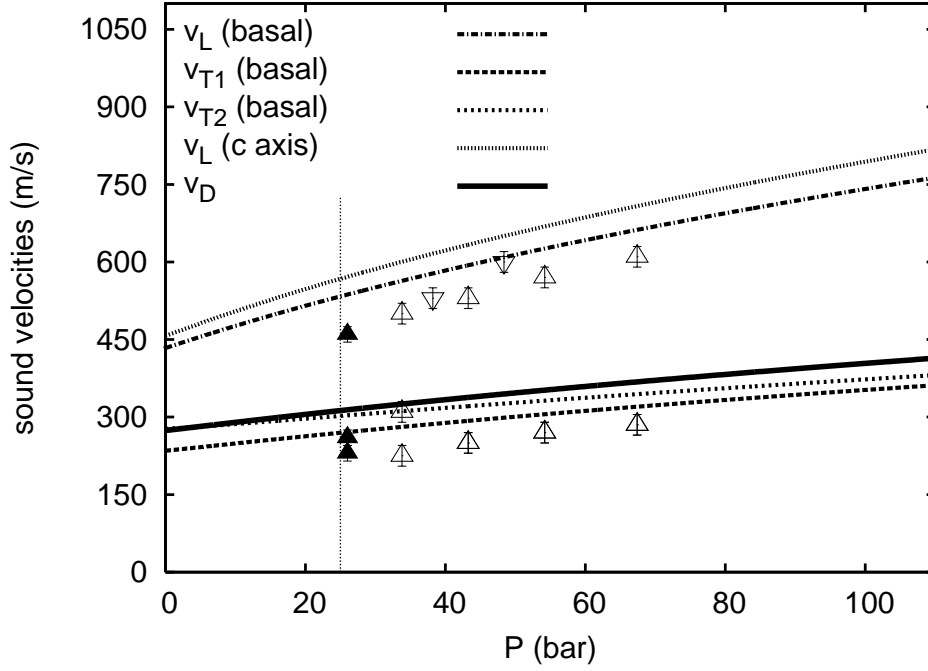


FIG. 6: Pressure dependence of the longitudinal (L) and transverse (T) sound velocities of hcp ^4He along its corresponding c -axis and basal plane. v_D represents the averaged Debye velocity (see text). Basal sound-velocity data from Refs. [3] (\triangle), [2] (\blacktriangle) and [1] (∇) are shown for comparison. The vertical dotted line represents the zero-temperature freezing pressure of ^4He .

amounts to zero since the atoms there remain frozen in their perfect lattice positions (that is, $C_{44}^p = C_{44}$). Even in the case of considering quasi-harmonic zero-point motion corrections to C_{44} , C_{44}^k is not expected to depart significantly from zero. In contrast, we found that in perfect hcp ^4He C_{44}^p/C_{44} amounts to 68 %, or conversely, $C_{44}^k/C_{44} = 32$ %. This last result quantifies the quantum nature of solid helium's elasticity and demonstrates the inability of classical and quasi-harmonic approaches for reproducing it.

B. Sound velocities

Sound velocities in solids, either longitudinal or transverse, depend on their direction of propagation. In crystals with hexagonal symmetry two main propagation modes are identified, one along the c -axis (defined by vector \mathbf{a}_3 in Section II A) and the other contained within the basal plane (defined by vectors \mathbf{a}_1 and \mathbf{a}_2 in Section II A). The relationships

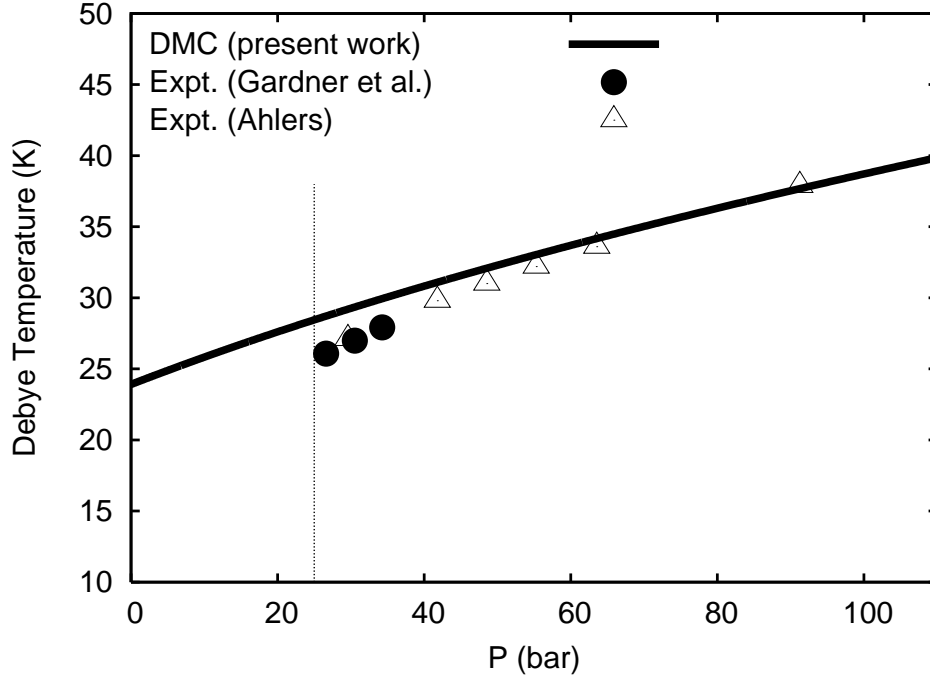


FIG. 7: $T = 0$ Debye temperature of hcp ^4He as a function of pressure (solid line). Experimental results from Refs. [51] and [52] are shown for comparison. The vertical dotted line represents the zero-temperature freezing pressure of ^4He , and the thickness of the line corresponds to the uncertainty associated to our calculations (e.g. $\delta\Theta_D/\Theta_D \sim 1\%$).

between the elastic constants and sound velocities in hcp crystals are^{48,49}

$$\begin{aligned}
 v_L &= (C_{33}/\rho)^{1/2} \\
 v_{T1} &= (C_{44}/\rho)^{1/2} \\
 v_{T2} &= (C_{44}/\rho)^{1/2}
 \end{aligned} \tag{14}$$

along the c -axis, and

$$\begin{aligned}
 v_L &= (C_{11}/\rho)^{1/2} \\
 v_{T1} &= (C_{66}/\rho)^{1/2} \\
 v_{T2} &= (C_{44}/\rho)^{1/2}
 \end{aligned} \tag{15}$$

within the basal plane.

In Fig. 6, we plot the pressure dependence of the tranverse and longitudinal sound velocities of hcp ^4He as obtained from our C_{ij} results reported in Section III A. The error

bars in our results, not shown in the figure, are $\delta v_{L,T}/v_{L,T} \sim 1\%$. It is observed that at compressions far beyond freezing all sound velocities increase almost linearly with pressure. In contrast, the longitudinal c -axis and basal components appear to follow a certain power-law within the low-density interval $0 \leq P \leq 25$ bars. Certainly, the nature of the sound propagation modes in metastable solid ^4He , either at positive or negative pressures, is poorly understood at present in spite of its fundamental physical interest.⁵⁰ It is our aim to report with detail on this topic in elsewhere so we leave discussions on this matter out of this work.

Experimental longitudinal and tranverse basal sound velocities are shown for comparison in Fig. 6. The agreement between those measurements and our predictions is generally good (in fact, as good as claimed in the previous section for the elastic constants). Specifically, our predicted sound velocities are systematically a bit larger than those values reported by Wanner¹, Crepeau² and Greywall.³ Such a systematic overestimation is consistent with our previous suggestion that certain thermal effects, non-reproducible by our simulations, could be affecting the experiments. As a fact of matter, the less rigid a material becomes by effect of temperature, the more slowly sound waves propagate across of it.

In order to provide a more meaningful comparison between our zero-temperature results and experiments, we computed the $T = 0$ Debye temperature of ^4He Θ_D . The zero-temperature Θ_D of a crystal can be easily extrapolated from lattice heat-capacity measurements performed at low temperatures, and results for this quantity have already been reported for helium over a wide pressure range.^{51,52} The definition of the $T = 0$ Debye temperature is

$$\Theta_D = \frac{2\pi\hbar}{k_B} \left(\frac{3}{4\pi V} \right)^{\frac{1}{3}} v_D, \quad (16)$$

where V is the volume per atom and v_D the Debye velocity. This velocity is given by

$$\frac{1}{v_D^3} = \frac{1}{3} \left(\frac{1}{\bar{v}_L^3} + 2\frac{1}{\bar{v}_T^3} \right), \quad (17)$$

where the average velocities \bar{v}_L and \bar{v}_T are defined by

$$\frac{1}{\bar{v}_{L,T}^3} = \langle \frac{1}{v_{L,T}^3} \rangle, \quad (18)$$

and the $\langle \dots \rangle$ brackets denote angular averages of the longitudinal and tranverse velocities.

In our case, we have approximated the angular averages in Eq. 18 by

$$\frac{1}{\bar{v}_L^3} \approx \frac{1}{2} \left(\frac{1}{v_{L,b}^3} \right) + \frac{1}{2} \left(\frac{1}{v_{L,c}^3} \right) \quad (19)$$

and

$$\frac{1}{\bar{v}_T^3} \approx \frac{1}{3} \left(\frac{1}{v_{T1,b}^3} \right) + \frac{1}{3} \left(\frac{1}{v_{T2,b}^3} \right) + \frac{1}{3} \left(\frac{1}{v_{T,c}^3} \right), \quad (20)$$

where index b stands for basal and index c for c -axis.⁵³

In Fig. 7, we plot our results for the zero-temperature Θ_D of hcp ^4He and experimental data taken from Refs. [51,52]. In fact, excellent agreement between Gardner and Ahlers measurements and our calculations is observed. This last result appears to further ratify our previous suggestion that, once thermal effects are corrected for, our $T = 0$ elastic constants and deriving quantities predictions closely reproduce experiments. Finally, we note that the pressure variation of Θ_D is very similar to that observed in the longitudinal sound-velocity components of helium, namely almost linear at high compressions and of power-law type at low densities.

IV. SUMMARY AND PERSPECTIVES

We have developed a fully quantum computational strategy to accurately calculate the zero-temperature elastic constants of perfect hcp ^4He under pressure. Our diffusion Monte Carlo results are shown to be consistent with low- T sound-velocity measurements and previous variational first-principles calculations. It is found that all five non-zero elastic constants of helium vary linearly with pressure within the range $0 \leq P \leq 110$ bar, and we have provided an accurate parametrization of each of them. The Grüneisen parameters, sound velocities and $T = 0$ Debye temperature of solid helium have been also determined and compared to experimental data. The computational method introduced in this work is totally general so that it can be used for the study of any other hcp quantum solid apart from helium (e.g. H_2), and/or be conveniently altered in order to investigate other crystal structures (e.g. face centered and body centered cubic).

It is our intention to analyze the elastic behavior of ^4He at negative pressures using the computational technique described here. In doing this, we expect to be able to determine its spinodal density limit (that is, the density at which the elastic constants vanish) rigorously, and also characterize the pressure dependence of the tranverse and basal sound velocities near it. Also we are interested in applying our formalism to the study of the ground-state of defective hcp ^4He (for instance, by introducing vacancies), where the supersolid state of matter clearly manifests. In doing this, we expect to gather quantitative knowledge on the

relationship (if any) between elasticity and supersolidity and so to help to understand the origins of recent shear modulus observations. Work in these directions is already in progress.

Acknowledgments

The authors acknowledge partial financial support from the DGI (Spain) Grant No. FIS2008-04403 and Generalitat de Catalunya Grant No. 2009SGR-1003.

-
- ¹ R. Wanner and J. P. Franck, Phys. Rev. Lett. **24**, 365 (1970).
² R. H. Crepeau, O. Heybey, D. M. Lee and S. A. Strauss, Phys. Rev. A **3**, 1162 (1971).
³ D. S. Greywall, Phys. Rev. A **3**, 2106 (1971); D. S. Greywall, Phys. Rev. B **16**, 5127 (1977).
⁴ J. Day and J. Beamish, Nature **450**, 853 (2007).
⁵ O. Syshchenko, J. Day and J. Beamish, J. Phys. Cond. Matt. **21**, 164204 (2009).
⁶ E. Kim and M. H. W. Chan, Nature **427**, 225 (2004).
⁷ E. Kim and M. H. W. Chan, Science **305**, 1941 (2004).
⁸ J. Day, O. Syshchenko and J. Beamish, Phys. Rev. Lett. **104**, 075302 (2010).
⁹ J. Day, O. Syshchenko and J. Beamish, Phys. Rev. B **79**, 214524 (2009).
¹⁰ X. Rojas, A. Haziot, V. Bapst, S. Balibar and H. J. Maris, Phys. Rev. Lett. **105**, 145302 (2010).
¹¹ H. Choi, D. Takahashi, K. Kono and E. Kim, Science **330**, 1512 (2010).
¹² D. Y. Kim, H. Choi, W. Choi, S. Kwon, E. Kim and H. C. Kim, Phys. Rev. B **83**, 052503 (2011).
¹³ I. Iwasa, Phys. Rev. B **81**, 104527 (2010).
¹⁴ C. Cazorla and J. Boronat, J. Phys.: Condens. Matter **20**, 015223 (2008).
¹⁵ C. Cazorla and J. Boronat, Phys. Rev. B **77**, 024310 (2008).
¹⁶ J. Boronat, C. Cazorla, D. Colognesi and M. Zoppi, Phys. Rev. B **69**, 174302 (2004).
¹⁷ C. Cazorla and J. Boronat, J. Low Temp. Phys. **134**, 43 (2004).
¹⁸ C. Cazorla and J. Boronat, Phys. Rev. B **78**, 134509 (2008).
¹⁹ C. Cazorla, G. Astrakharchick, J. Casulleras and J. Boronat, J. Phys.: Condens. Matter **22**, 165402 (2010).
²⁰ R. Pessoa, S. A. Vitiello and M. de Koning, Phys. Rev. Lett. **104**, 085301 (2010).

- ²¹ C. Cazorla, E. Sola and D. Errandonea, Phys. Rev. B **80**, 064105 (2009).
- ²² G. Steinle-Neumann, L. Stixrude and R. E. Cohen, Phys. Rev. B **60**, 791 (1999).
- ²³ C. Cazorla, D. Alfè and M. J. Gillan, Phys. Rev. Lett. **101**, 049601 (2008).
- ²⁴ M. J. Gillan, D. Alfè, J. P. Brodholt, L. Vocadlo and G. D. Price, Rep. Prog. Phys. **69**, 2365 (2006).
- ²⁵ S. Baroni, S. de Gironcoli, A. del Corso and P. Giannozzi, Rev. Mod. Phys. **73**, 515 (2001).
- ²⁶ D. Alfè, Comput. Phys. Comm. **180**, 2622 (2009).
- ²⁷ G. Kresse, J. Furthmüller and J. Hafner, Europhys. Lett. **32**, 729 (1995).
- ²⁸ T. H. K. Barron and M. L. Klein, Proc. Phys. Soc. **85**, 523 (1965).
- ²⁹ D. C. Wallace in *Thermodynamics of Crystals*, New York, Wiley (1972).
- ³⁰ W. F. King and P. H. Cutler, J. Phys. Chem. Solids **32**, 761 (1970).
- ³¹ B. L. Hammond, W. A. Lester and Jr. P. J. Reynolds in *Monte Carlo Methods in Ab Initio Quantum Chemistry*, World Scientific, Singapore (1994).
- ³² R. Guardiola, Lecture Notes in Physics **510**, 269 (1998).
- ³³ D. M. Ceperley and M. H. Kalos in *Monte Carlo methods in statistics physics*, Springer-Verlag, Berlin (1986).
- ³⁴ By related quantities is meant the expected value of operators \hat{A} that commute with the Hamiltonian, namely $[\hat{A}, \hat{H}] = 0$. It is also possible to obtain virtually exact results for some particular $[\hat{A}, \hat{H}] \neq 0$ operators by using forward walking based techniques (see Refs. [35] and [36]).
- ³⁵ R. Barnett, P. Reynolds and W. A. Lester Jr., J. Comput. Phys. **96**, 258 (1991).
- ³⁶ J. Casulleras and J. Boronat, Phys. Rev. B **52**, 3654 (1995).
- ³⁷ R. A. Aziz, F. R. W. McCourt, and C. C. K. Wong, Mol. Phys. **61**, 1487 (1987).
- ³⁸ J. Boronat and J. Casulleras, Phys. Rev. B **49**, 8920 (1994).
- ³⁹ C. Cazorla, G. Astrakharchick, J. Casulleras and J. Boronat, New Journal of Phys. **11**, 013047 (2009).
- ⁴⁰ M. C. Gordillo, C. Cazorla and J. Boronat, Phys. Rev. B **83**, 121406(R) (2011).
- ⁴¹ S. A. Chin, Phys. Rev. A **42**, 6991 (1990).
- ⁴² Y. Lutsyshyn, C. Cazorla, G. E. Astrakharchik and J. Boronat, Phys. Rev. B **82**, 180506(R) (2010)
- ⁴³ Y. A. Freiman, S. M. Tretyak, A. Grechnev, A. F. Goncharov, J. S. Tse, D. Errandonea, H.-K. Mao and R. J. Hemley, Phys. Rev. B **80**, 094112 (2009).

- ⁴⁴ S. Vitiello, K. Runge and M. H. Kalos, Phys. Rev. Lett. **60**, 1970 (1988).
- ⁴⁵ S. Moroni, D. E. Galli, S. Fantoni and L. Reatto, Phys. Rev. B **58**, 909 (1998).
- ⁴⁶ M. L. Klein, G. Chell, V. V. Goldman and G. K. Horton, J. Phys. **C3**, 806 (1970).
- ⁴⁷ J. B. Lurie, J. Low Temp. Phys. **10**, 751 (1973).
- ⁴⁸ M. J. P. Musgrave, Proc. R. Soc. Lond. A **226**, 339 (1954).
- ⁴⁹ V. V. Goldman, J. Low Temp. Phys. **36**, 521 (1979).
- ⁵⁰ H. J. Maris, J. Low Temp. Phys. **155**, 290 (2009).
- ⁵¹ W. R. Gardner, J. K. Hoffer, and N. E. Phillips, Phys. Rev. A **7**, 1029 (1973).
- ⁵² G. Ahlers, Phys. Rev. A **2**, 1505 (1970).
- ⁵³ In view of the experimental results reported in Fig. 10 of Ref. [3], this approximation can be considered as certainly good.